VDMA
Fluid Power Association

23rd ISC

International Sealing Conference

Stuttgart, Germany
Sept.30 - Oct.1, 2026

Sealing the future –
Facing the challenges of tomorrow

UNI STUTTGART

Fachverband Fluidtechnik im VDMA e. V. Lyoner Str. 18
50628 Frankfurt am Main
Germany

Phone +49 69 6603-1513
E-Mail maximilian.baxmann@vdma.eu

Internet www.vdma.eu/fluid

Numerical and Experimental Investigation of Calotte-Microstructured Shaft Counter-Surfaces for Radial Shaft Seals

Lenine M. de C. Silva, Thomas Junge, Olaf Grutza, Andreas Nestler, Stefan Thielen, Oliver Koch, Andreas Schubert

Radial shaft seals are used in rotary shaft applications to prevent the leakage of lubricants. In addition to the characteristics of the sealing lip, the shaft counter surface influences the tribological behaviour of the sealing system. In this study, calotte shaped microstructured shaft surfaces are analysed experimentally and by hydrodynamic simulation to quantify their contribution to the axial pumping rate of the sealing system. The structures were manufactured using a two-stage longitudinal turning process. First, a periodic microstructure was created by ultrasonic-assisted turning, after which the surface was machined to its final contour in a second turning step and finally characterised geometrically. In addition, the structure formation was simulated kinematically, with the resulting surfaces being used as input for the hydrodynamic simulation model. Experimentally, the pumping rate of the shaft counter surface was determined using a two-chamber test rig and by isolating the respective contributions of the shaft and seal through a change in the rotational direction. In addition, the pumping rates of the simulated surfaces were calculated using a hydrodynamic simulation based on the Reynolds equation, with the complementarity conditions formulated via the Fischer-Burmeister function. The findings show that calotte structures measurably influence the pumping rate of the shaft counter surface. The experimental and numerical results display corresponding qualitative trends, with the simulation serving as a comparative tool for evaluating structure-induced hydrodynamic effects. A sensitivity analysis of the lubricant film thickness suggests that its influence is geometry dependent and can affect both the magnitude and direction of axial fluid transport. The results therefore show that calotte shaped microstructured shafts can be used to modify the fluid transport in the radial shaft seal contact.

1 Introduction

Radial shaft seals (RSS) are commonly used to prevent oil leakage in rotary shaft applications under relative motion between the seal and the shaft counter surface (SCS) [1]. The RSS is press-fitted into the housing, establishing a static sealing function at its outer diameter. During installation, the sealing lip is elastically expanded due to its radial interference with the shaft and tilts towards the air side. Owing to the sealing edge geometry, in particular the different contact angles α (at the oil side) and β (at the air side), an asymmetric contact pressure distribution develops supported by a garter spring, with maximum contact pressure shifted to the oil side, which ensures sealing conditions without shaft rotation [2]. During operation, this pressure distribution leads to a deformation of the sealing lip surface structure, comprised of roughness [3] and adhesion-induced folds [4] (see Figure 1).

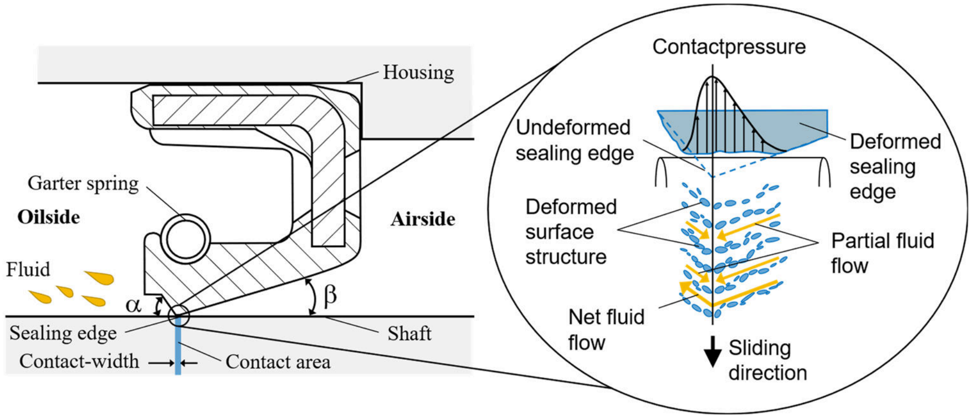

Figure 1: Radial shaft sealing system (left) and distortion based sealing mechanism (right) based on /1, 5/

The oil entrained in the circumferential direction is redirected towards the pressure maximum by the resulting V-shaped surface structure [6]. With a predominant flow directed to the oil side, a net reverse pumping effect is established. This distortion model, based on the elastic properties of the sealing lip, is regarded as the predominant sealing mechanism of RSS [3], [6], [7].

In addition to this sealing mechanism of RSS, the shafts surface characteristics significantly influence the performance of the sealing system. For example, overly smooth shaft surfaces or lead structures may cause leakage [7]. The latter are surface features that contribute as an additional shaft-induced axial flow component of the sealed fluid [8], which is superimposed on the reverse pumping effect of the RSS. The pumping effect of the RSS and shaft can be separated and investigated using different experimental setups [9]. The shaft surface condition is also relevant for the friction torque generated between the shaft and the seal as a result of their relative motion [10], [11], [12]. For instance, compared with ground shafts, lower friction torque has been observed for turned countersurfaces with circumferential roughness features, which can act as lubricant reservoirs [13]. Such reservoirs can also be introduced by targeted micro texturing of the shaft surface in order to improve the tribological behaviour [9], [10], [14]. However, such surface structures can also have a significant influence on the reverse pumping effect of the sealing system [10], [11], [15].

The influence of targeted microstructuring of surfaces on the sealing system has been investigated in the past both experimentally /12, 15, 16/ and through simulation [12], [17], [18], [19]. The focus has primarily been on deterministic structures such as triangular, rectangular, or circular indentations and protrusions with constant depth or thickness. Most studies deal with the microstructuring of the shaft [10], [12], [15], [16], [20], while only a few consider microstructuring of the seal [19], [21]. The microstructures used in the experiments were mostly created by laser ablation [18], [19] or electroplating [15]. STEINERT ET AL. have already designed specific functional, deterministic surface microstructures and manufactured them using ultrasonic vibration-assisted face turning [22], [23], [24]. In this context, two-stage turning proved particularly suitable for machining of calotte-shaped microstructures on bronze bodies. In subsequent tribological investigations, this approach enabled a reduction in the coefficient of friction of lubricated steel-bronze sliding pairs.

Before target-microstructured SCS can be employed in RSS systems, their influence on the sealing system must first be understood. Reliable prediction of the hydrodynamic (HD) behaviour of target-microstructured SCS under operating conditions representative of practical RSS applications is therefore required. Consequently, this work aims to develop and experimentally validate a HD numerical model capable of predicting the hydrodynamic contribution of the shaft counter surface to fluid transport within the sealing contact.

2 Materials and methods

The reverse pumping rate of different structured counter surfaces is investigated both experimentally and numerically. Section 2.1 details the modelling and manufacturing of the structured shafts. Section 2.2 describes the experimental setup and measurement procedure, whereas Section 2.3 outlines the numerical framework.

2.1 Calotte-Microstructured Shaft Counter-Surfaces

A simulation model developed in MATLAB software and first introduced for vibration-imposed milling in [25] and [26] was extended to predict and evaluate the kinematic surface structure during two-stage turning. This kinematic approach subtracts the tool geometry from the workpiece surface along the tool trajectory in discrete time steps, but does not consider elastic-plastic effects, such as burr formation or thermal expansion. The result of the kinematic simulation is a point cloud of the ideal surface structure measuring 1 mm² with a lateral resolution of 1 µm in the x and y directions (Figure 2a).

To characterize the HD performance of target-microstructured SCS in RSS systems, the surfaces were manufactured by longitudinal hard turning using a two-step machining process to generate the targeted microstructures on the SCS. For the experimental investigations specimens of the alloyed steel 16MnCr5 in the case-hardened condition (55+5 HRC, hardening depth approx. 1 mm) were processed. The geometry was characterized by a diameter of 40 mm, a length of 18.5 mm and an axial bore with a diameter of 26 mm that is utilized for clamping by a mandrel.

The machining process for the manufacturing of the calottes required two stages. In each case, CBN tipped indexable inserts were used. The tools were characterized by a tool included angle of 80° and a rake angle of 0°. Figure 2b depicts the resulting surface microstructure and its geometrical parameters.

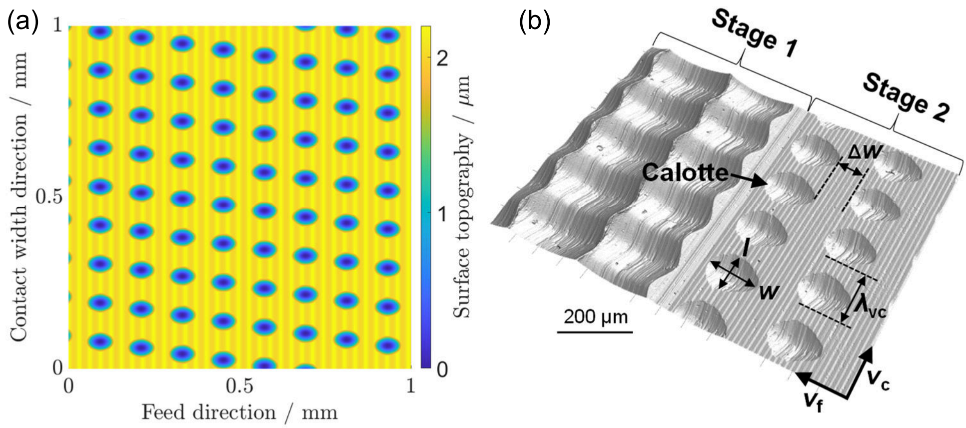

Figure 2:(a) Microstructured surface in top view; (b) Resulting surface microstructure of process stage 1 and 2 and the geometrical parameters of the calottes

The machining was carried out on a precision lathe SPINNER PD 32 in an air-conditioned laboratory with a constant temperature of 20°C. In a first process stage, the tool kinematics during external longitudinal turning was super-imposed with a high-frequency oscillation in the ultrasonic range (24.3 kHz resonance frequency) perpendicular to the specimen surface. The vibration of the tool created a micro-structured surface which exhibited a sinusoidal profile in the cutting direction. It is important that the flank face does not intersect with this wavy surface structure. Therefore, a clearance angle of 15° was chosen for the tool of the first process stage.

In the second process stage, machining was carried out without the superimposition of an ultrasonic vibration, whereby the depth of cut was selected to be smaller than the microstructure depth generated in the first process stage. The result is a plateau-like surface with distinct cavities, which are referred to as calottes. Since the depth of cut was very small during the second process stage, a relatively sharp CBN tool with a cutting-edge radius of approximately 4 µm and a clearance angle of 7° was applied. The machining conditions for the second process stage remained constant for all microstructures with a cutting speed of 180 m/min and a feed of 0.03 mm. The radial position of the tool in reference to the specimen was the same as in the first process stage.

The resulting calottes were varied in terms of their areal size (width, length), spacing and depth. These geometric parameters depended on the corner radius of the tool, the amplitude and frequency of the ultrasonic oscillation (24.3 kHz) as well as the cutting parameters feed and cutting speed. The following Table 1 summarizes the resulting microstructure parameters.

Table 1: Theoretical microstructure parameters of the calottes after two-stage turning

Parameter	Microstructure variants			
	1	**2**	**3**	**4**
Depth d / µm	2	4	4	4
Width w / µm	80	80	113	113
Length l / µm	56.5	56.5	56.5	80
Distance Δw / µm	40	40	40	40
Distance λ_{vc}* / µm	113	113	113	160
Lead Angle / °	0.01413			

*The variation of λ_{vc} is indirectly dependent on the length l

2.2 Experimental setup for determining the reverse pumping rate

The test setup used to determine the reverse pumping rate of the sealing system and its components is depicted in Figure 3. It is based on the two-chamber method introduced by KUNSTFELD [9] and applied for example by BURKHART [27]. In this configuration, the RSS is mounted between the two chambers and separates them from one another. For the presented pumping rate measurements both chambers are completely filled with the test lubricant and are equipped with riser pipes. To monitor the hydrostatic pressure, both chambers are equipped with high resolution pressure sensors. At the beginning of the test, the riser pipe of chamber 2, corresponding to the RSS air side, is fully filled with the lubricant to an initial pressure of 43.7±1.3 mbar, whereas the riser pipe of chamber 1, corresponding to the oil side, was filled up to 22.5±2.5 mbar was reached at the measurement level.

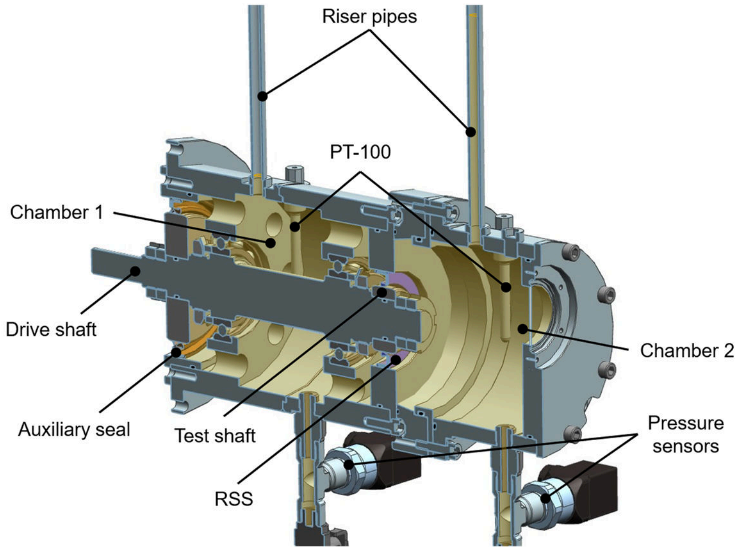

Figure 3: Sectional view of the two-chamber test rig for pumping rate measurement

The pumping rate PR of the sealing system can be calculated according to Equation (1) from the gradient of the pressure change K, the riser pipe diameter d_{RP}, the lubricant density at sump temperature $\rho_{70°}$, the relative speed v_{rel} between the RSS and the shaft in the contact zone and the gravitational acceleration g.

$$PR = \frac{|K| {d_{RP}}^2 \pi}{4\rho_{70°} g v_{rel}} \tag{1}$$

As described in Section 1, the pumping rate of the shaft and the RSS are superimposed. Following the approach of BURKHART [27] based on RAAB [28], the pumping rates of the shaft PR_{Shaft} and the RSS PR_{Seal} can be separated and determined by carrying out the pumping rate measurements for the sealing system in both directions of rotation: positive (PR_{POS}) and negative (PR_{NEG}). As illustrated in Figure 4, both component specific pumping rates are derived from the direction dependent total pumping rates of the sealing system.

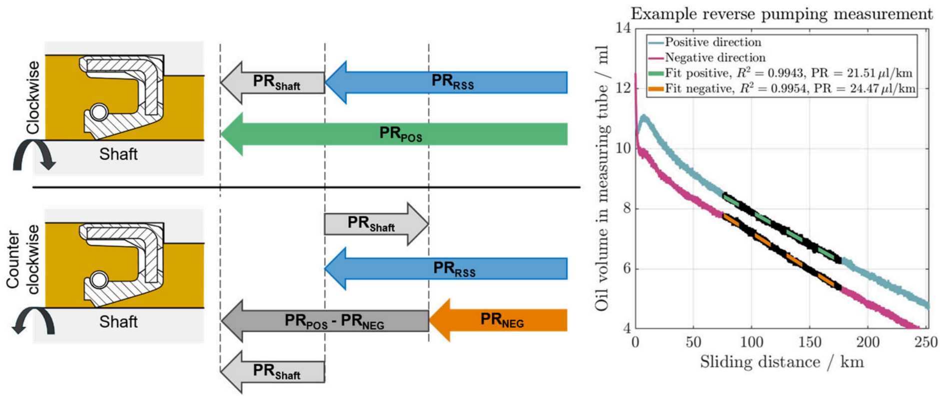

Figure 4: Measurement technique and separation of the component-specific pumping rates of RSS and shaft surface based on [27] according to Raab [28]

Although the pumping rate of the RSS can be affected by direction dependent conditioning, replacing the RSS within a measurement series would introduce additional influences on the measured pumping rate. These influences may result from tolerances in features such as seal geometry and radial force, as well as from variations in the positioning of the sealing lip on the wear-track. For this reason, the RSS was not replaced within a measurement series. The seals pumping rate PR_{Seal} is here assumed to be independent of the rotational direction. Based on this assumption, it can be calculated using Equation (2).

$$PR_{Seal} = \frac{1}{2}(PR_{POS} + PR_{NEG}) \tag{2}$$

For the shaft, the direction dependent pumping rate PR_{Shaft} is calculated according to Equation (3).

$$PR_{Shaft} = \frac{1}{2}(PR_{POS} - PR_{NEG}) \tag{3}$$

This method and evaluation are only valid if the condition $PR_{Shaft} < PR_{Seal}$ is met, which applies to all measurements considered in this study. Otherwise, the pumping rate of the shaft would be underestimated.

All measurements were conducted at a rotational speed of 2,000 rpm and an oil sump temperature of 70 °C, which was maintained in both chambers by PID-controlled heating systems. Each surface variant was evaluated using two shaft specimens. Every specimen was tested successively in the positive and negative directions of rotation under identical operating conditions. Each rotational direction was continued until the pressure in the air-side chamber decreased to approximately 12 mbar, indicating that the oil level had nearly reached the bottom of the measuring tube. The investigated sealing system consisted of a BAUM3X7 RSS (40 × 60 × 10 mm) made of 75 FKM 585, lubricated with a PAO, ISO VG 46, v = 38.9 / 9.2 mm²/s (40 / 100 °C).

2.3 Simulation model for the reverse pumping rate

A HD-simulation was used to evaluate the extent to which the given structured SCS contribute to the pumping rate of the sealing system by calculating the direction and magnitude of the lubricant transport in each discretization point [29]. The respective shaft structure is implemented into the model as the local gap geometry, while the sealing lip is modelled as a smooth, rigid counterpart. This specifically isolates the influence of the SCS. The local lubricant gap height is defined by superimposing a prescribed offset onto the topography of the SCS, whereby its influence on the pumping rate was examined through variation as part of a sensitivity analysis (varying between 0.8 and 1.4 µm [30]). Roughness of the sealing edge as well as elastic deformations of the sealing contact, mixed friction and wear or run-in effects are not considered.

The calculation is based on the REYNOLDS equation for thin lubricant films utilizing a mass-conserving cavitation model in accordance with WOLOSZYNSKI [31], in which a cavitation degree is introduced in addition to the pressure field and coupled to the pressure via a FISCHER-BURMEISTER condition. The local flow components are derived from the numerically determined pressure and cavitation distributions and combined to obtain the volumetric flow rate. Relative motion is not modelled by a transient translation of the topography, but by the velocity terms in the Reynolds equation.

The simulated topography of each shaft counter surface was directly imported into the numerical model to define the local lubricant film geometry. The shaft diameter and rotational speed were chosen identical to the experimental conditions (40 mm and 2,000 rpm, respectively). Likewise, the same lubricant (PAO, SAE 0W20) and its temperature-dependent material properties were adopted in the simulations.

The computational domain consisted of a square section of the simulated topography with dimensions ranging from approximately 0.35 × 0.35 mm² to 0.45 × 0.45 mm², depending on the structural variant. The domain size was selected to avoid truncating individual calottes at the domain boundaries, which was found to improve the numerical stability of the simulations. Consequently, the computational domain contained between 2 × 2 and 3 × 4 calottes, depending on the respective surface structure. The topography was discretized using a uniform Cartesian mesh with a grid spacing of 0.4 µm in both the circumferential and axial directions.

An initial pressure field of 3 MPa was prescribed over the complete computational domain to initialize the iterative solution procedure. Lubricant viscosity and density were evaluated using temperature-dependent material models, including a VOGEL viscosity correlation. The nonlinear REYNOLDS–FISCHER–BURMEISTER system was solved iteratively using a GAUSS–SEIDEL scheme with an under-relaxation factor of 0.3. The iterative solution was considered converged when the convergence criterion reached 1×10^{-6}. For numerical stability, the governing equations were solved in dimensionless form, while all results are reported in physical units.

The results should be interpreted as comparative hydrodynamic parameters for the structural variants investigated, not as a comprehensive system prediction for RSS. The validity of the model is limited by the assumptions of the REYNOLDS theory, in particular narrow lubrication gaps and no significant pressure gradients across the film height. For deep structures, recirculation and inertia may dominate the pressure distribution, requiring analysis based on the STOKES or NAVIER-STOKES equations [32].

The simulation results are therefore interpreted not as absolute values but as a comparative parameter for the functional effect of the shaft structures and are assessed against the experimentally determined pumping rates.

3 Results and Discussion

This section presents the experimental and numerical results. Section 3.1 describes the geometric characterization of the manufactured SCS. Section 3.2 presents the experimental reverse pumping rates. Section 3.3 presents the numerical results and compares them to the experimental results.

3.1 SCS Manufacturing

Upon the manufacturing phase, the lateral dimensions of the microstructures and their spacing between each other were measured with an optical microscope (Keyence VHX-X1). To determine the depth and surface roughness accurately, additional measurements were conducted by an optical coordinate measuring machine (Bruker alicona µCMM). The measurement data was processed according to DIN 25178.

To distinguish between the depth of the valleys and the roughness of the plateau the functional parameters reduced peak height *Spk*, core roughness depth *Sk* and reduced valley depth *Svk* were applied. They are also known as bearing capacity parameters and determine the functional properties, particularly in terms of tribology and lubrication. Their calculation is based on the areal material ratio curve, but is only applicable to surfaces with distinct cavities (e.g. lapped, ground, or honed surfaces). *Spk* describes the mean height of peaks above the core surface. These peaks are typically removed during the run-in phase. *Sk* is the core roughness depth that characterizes the actual roughness of the surface plateau with which the sealing ring is in contact. *Svk* refers to the valley depth below the core roughness and indicates the depth of the area where lubricant can be stored (Table 2).

Table 2: Measured geometrical parameters of the manufactured SCS

Parameter	**Microstructure variants**			
	1	**2**	**3**	**4**
Sk + *Spk*[1] / µm	1.7	1.7	2.1	2.1
Svk[2] / µm	1.6	3.1	4	4.5
Width *w* / µm	72	74	108	119
Length *l* / µm	54	53	64	89
Distance Δw / µm	47	45	44	34
Distance λ_{vc} / µm	111	113	113	158

[1] roughness of the surface plateau; [2] depth of the calottes

The geometric deviations between the theoretical and measured microstructures can be attributed to slight tool wear, minor deviations in the alignment of the tools from process stage 1 and 2 (relative to each other), along with variations in the tool corner geometry (slightly smaller corner radius) within the manufacturer's tolerance.

To allow for a better interpretation of the subsequent tribological test results, plunge grinded SCS (surface roughness *Ra* = 0.15 µm, *Rz* = 1.15 µm) as well as exclusively hard-turned SCS (surface roughness *Ra* = 0.29 µm, *Rz* = 1.33 µm) were machined.

3.2 Experimental Reverse Pumping Measurements

Since each shaft specimen was tested in both the positive and negative directions of rotation and two specimens were investigated for each surface variant, four reverse pumping curves were obtained for every variant. As described in Figure 4, each measured reverse pumping rate represents the combined pumping behaviour of the RSS and the corresponding SCS.

The calculation of the individual reverse pumping rates, separating the contributions of the RSS and the SCS, as described in Section 2.2, was applied to the measured data in order to quantify the hydrodynamic contribution of each component to the overall reverse pumping rate. The resulting individual pumping rates of the RSS and the SCS for all investigated variants are presented in Figure 5a.

Since two shaft specimens were tested for each surface variant, the mean reverse pumping contribution of each variant was determined as the arithmetic mean of the two individual measurements. The resulting ranking of the mean reverse pumping rates for all investigated surface variants is shown in Figure 5b.

It is initially observed that the reverse pumping values for the RSS vary considerably, even though the RSS specimens used are of the same model and have identical dimensions. The reverse pumping values among the SCS specimens for each variant, despite there being only two samples per variant, show considerably less variation. Furthermore, the reverse pumping value appears to be proportional to the depth of the calotte the reference SCS exhibits reverse pumping close to zero, while Variant 1, featuring less deep calottes, shows the second-lowest reverse pumping value. Variants 2, 3, and 4 have similarly deeper calottes and exhibit higher reverse pumping values.

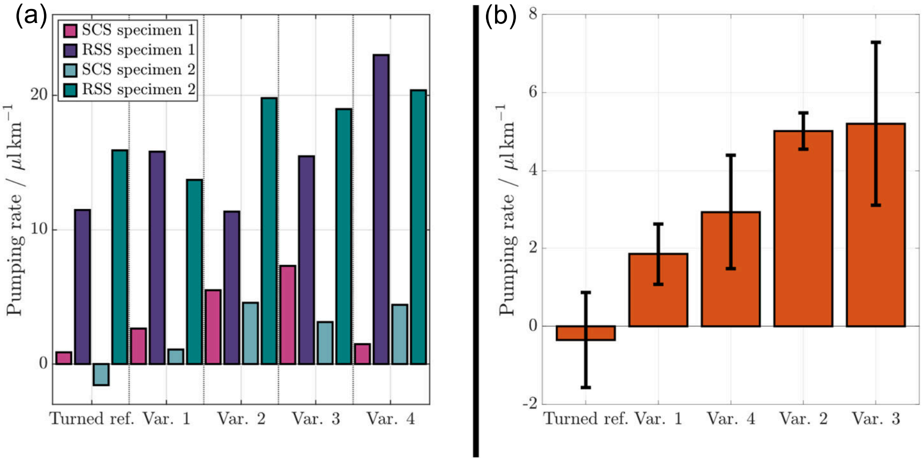

Figure 5: (a) Reverse pumping rate by surface variant; (b) Ranking of mean SCS pumping rate.

3.3 Hydrodynamic Model Predictions

The simulation's result is a pressure distribution over the shaft counter surface (Figure 6a). Based on this pressure field, together with the local sliding velocity and the lubricant properties, the local volumetric flow distribution is calculated for the entire computational domain (Figure 6b).

Analogous to the experimentally determined reverse pumping rate, the numerical pumping rate has to be evaluated along a line parallel to the circumferential direction. However, the presence of calotte structures results in a highly non-uniform local flow distribution. Consequently, selecting an arbitrary evaluation line may lead to a pumping rate that is not representative of the overall hydrodynamic behaviour of the structured surface.

To obtain a representative pumping rate, the axial volumetric flow was evaluated over the complete computational surface. Since the local flow within the calottes is dominated by internal recirculation and REYNOLDS simulation's process is not capable of simulating a three-dimensional flow behaviour, all surface regions corresponding to the calottes were excluded from the evaluation [32].

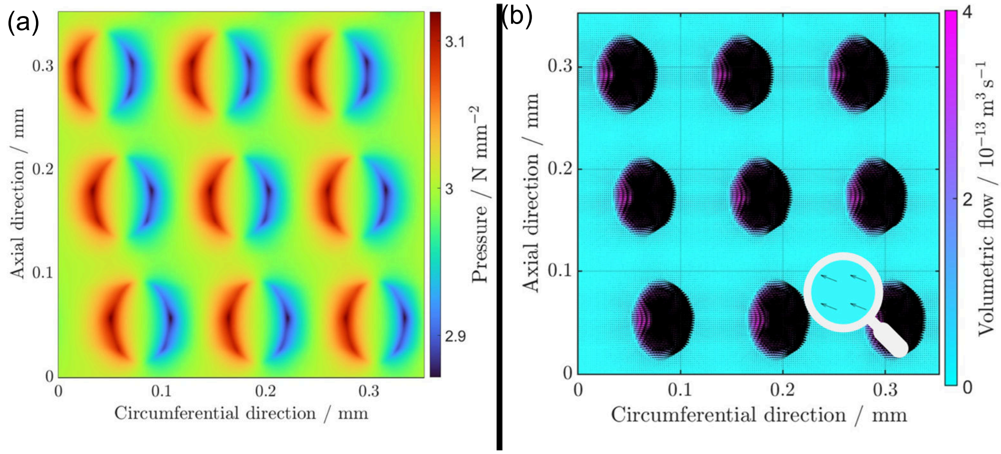

Figure 6: (a) Pressure distribution over the lubricant filme; (b) Volumetric flow distribution.

Since each variant has over 800 profiles along the axial direction, mean and median axial volumetric flow of the remaining surface area were used as representative measures of the hydrodynamic pumping effect of each surface variant. The simulation results are evaluated together with the corresponding experimental results in Figure 7.

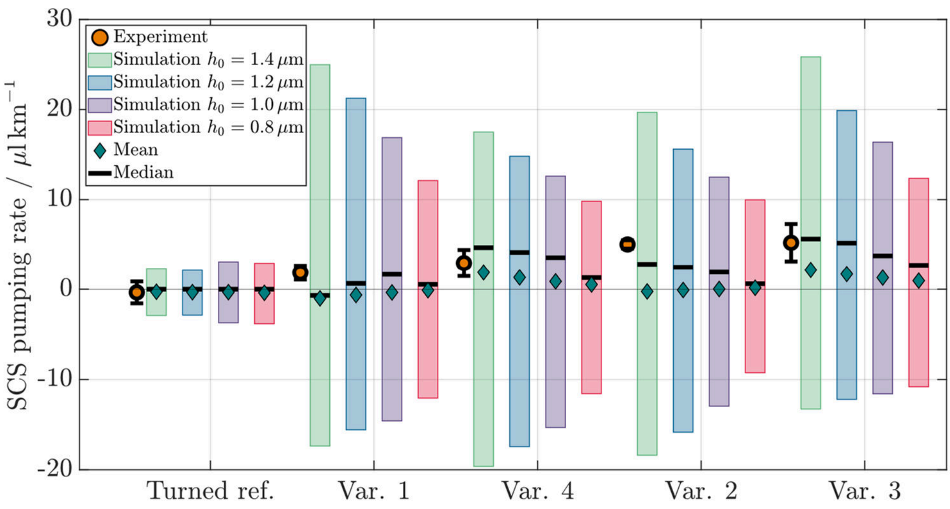

Figure 7: Results comparison between experiment and HD simulation.

3.4 Discussion and Outlook

The experimental and numerical results show that the microstructured SCS measurably influence the pumping rate of the investigated sealing systems and suggest, that calotte structures effect lubricant film formation. However, the results should be interpreted as a comparative evaluation of structured shaft counter surfaces rather than as absolute predictions of pumping performance. The experimentally determined pumping rates show distinct variations typically for RSS. Furthermore, the evaluation of the RSS and shafts pumping rates assumes that the flow contribution of the RSS is direction-independent and that the respective pumping rates of both constituents are completely decoupled. This assumption is appropriate for the chosen analysis. Furthermore, the objective of the present HD model is not to reproduce the complete sealing contact but to isolate and evaluate the hydrodynamic contribution of the SCS to the lubricant transport. In the present HD model, the lubricant film thickness is prescribed as an input parameter rather than being calculated. Consequently, a sensitivity analysis was performed to evaluate its influence on the predicted hydrodynamic pumping behaviour.

Despite these limitations, the simulation and experiment show similar qualitative trends. The only discrepancy between the experimental ranking and the numerical prediction is observed for Variants 2 and 4, whose positions are interchanged. This difference may be related to the experimental scatter, the computational representation of Variant 4, or a combination of both effects. The simulation therefore appears to provide a suitable tool for estimating structure-based differences and identifying general trends in hydrodynamic pumping behaviour. Although discrepancies between the simulated and measured pumping rates remain, the sensitivity analysis showed that the numerical predictions approach the experimentally measured values for lubricant film thicknesses within the range reported in the literature [30]. Since experimental information on lubricant film thickness in RSS contacts is limited in the literature, some uncertainty remains in the quantitative comparison. Here it is noticeable that the simulated flow rates do not respond uniformly to an increase in the specified lubrication film thickness across the investigated variants.

The local volumetric flow generated by the calotte structures is highly non-uniform over the computational surface. Consequently, the distribution of the axial flow obtained from the individual profiles cannot be adequately characterized by a single statistical measure. Therefore, both the mean and the median flow rates were considered to obtain a more comprehensive description of the hydrodynamic behaviour of each surface variant.

For two of the investigated variants (Variants 2 and 4), both the mean and the median pumping rates increase with higher lubricant film thickness, indicating a consistent hydrodynamic response throughout the evaluated surface. Variant 1 exhibits a different behaviour. Both statistical measures show an increasing pumping effect with higher lubricant film thickness; however, this increase occurs in the negative direction of the flow. Since Variant 1 already generates a negative pumping rate for the smallest investigated film thickness, the progressively more negative values indicate an increase in the magnitude of the reverse pumping effect rather than a reduction of its hydrodynamic performance.

Variant 2 exhibits the most complex behaviour. While the mean pumping rate changes from positive to negative values with increasing lubricant film thickness, suggesting a reversal of the overall flow direction within the investigated range, the median simultaneously shifts towards more positive values. This indicates that the global mean is strongly influenced by localized regions exhibiting pronounced pumping, whereas the majority of the surface follows the opposite trend. Consequently, the hydrodynamic behaviour of Variant 2 cannot be adequately interpreted from the mean pumping rate alone and requires consideration of both statistical measures.

Future experimental work should include additional shaft variants with varying calotte parameters (depth, width, length, spacing) in order to isolate and determine the key factors influencing the pumping rate. Subsequent simulation studies should include additional sensitivity analysis, especially of the topography section under consideration. The presented calculations contain a limited number of calottes. As a result, effects of the topography edges as well as the specific location of the section may influence the calculated pumping rates.

4 Summary and Conclusion

In the present study, calotte-microstructured shaft counter surfaces for radial shaft seals were manufactured and investigated experimentally as well as numerically with regard to their influence on the shafts pumping rate. The surfaces were produced using a two-stage longitudinal turning process, geometrically characterized and additionally modelled through a kinematic simulation of the structure formation. The simulated topographies were then used as input parameters for a hydrodynamic simulation. The pumping rates were experimentally determined using a two-chamber test bench and separated into seal and shaft components. The key findings are as follows:

- The calotte shaped structures examined have a measurable effect on the shafts pumping rate. The experiment and HD simulation show comparable qualitative trends for the shaft variants examined. The observed differences between the reference and structural variants demonstrate that the calotte structures influence axial fluid transport. An effect on local lubricant formation is therefore likely.
- The sensitivity analysis demonstrates that the hydrodynamic response of calotte-structured surfaces to increasing lubricant film thickness might be geometry-dependent. The observed differences between the investigated variants indicate that the interaction between surface topography and lubricant film thickness may govern the intensity of pumping effect and also the direction of the flow. The influence of lubricating film height must therefore be investigated as part of further sensitivity studies (for example by using a TEHD simulation).
- To better describe the pumping behaviour of the structured surfaces, different parameters of the axial flow components were analysed. In addition to the mean value, which describes the resulting flow contribution of the topographic section under investigation, the median was used to characterise the spatial distribution of the local flow components. Differences between the two parameters show that

the flow behaviour of the calotte structures is not distributed homogenously across the surface but is characterized by flow components that vary in intensity.

The results thus show that, within the limits of the model, the HD simulation can be a suitable tool for comparative evaluation and optimization of structured shaft counter surfaces. However, this is contingent on the observed trends being confirmed by detailed TEHD simulations.

5 Acknowledgements

Funded by the Deutsche Forschungsgemeinschaft (DFG, German Research Foundation) - Project-ID 430170022 – TH 2587/3-3 and Project-ID 511263698 – TRR 375.

6 Nomenclature

Variable	***Description***	***Unit***
d_{RP}	Diameter of the riser pipe	[m]
g	Gravitational acceleration	[m/s^2]
PR	Pumping rate of the sealing system	[µl/m]
PR_{Seal}	Pumping rate of the seal	[µl/m]
PR_{Shaft}	Pumping rate of the shaft	[µl/m]
K	Gradient of the pressure slope	[Pa/s]
v_{rel}	Sliding speed in contact zone	[m/s]
α	Surface Pressure	[rad]
β	Temperature	[rad]
$\rho_{70°}$	Lubricant density at operating temperature	[kg/m^3]

Symbol	***Description***
FKM	Fluorelastomer
NEG	Negative
PAO	Polyalphaolefin oil
PID	Proportional, integral, and derivative
POS	Positive
RSS	Radial shaft seal
SCS	Shaft counter surface

7 References

[1] H. K. Müller, B. S. Nau and B. S. Nau, Fluid sealing technology, New York, NY [u.a.]: M. Dekker, 1998.

[2] B. Sauer, Ed., Konstruktionselemente des Maschinenbaus 2: Grundlagen von Maschinenelementen für Antriebsaufgaben, Springer Berlin Heidelberg, 2025.

[3] L. Horve, Shaft seals for dynamic applications, New York, NY [u.a.]: Dekker, 1996.

[4] A. Schallamach, "How does rubber slide?" *Wear,* vol. 17, p. 301–312, April 1971.

[5] A. Riedl, Ed., Handbuch Dichtungspraxis, 4. Auflage ed., Essen: Vulkan Verlag, 2017.

[6] R. F. Salant, "Theory of lubrication of elastomeric rotary shaft seals" *Proceedings of the Institution of Mechanical Engineers, Part J: Journal of Engineering Tribology,* vol. 213, p. 189–201, March 1999.

[7] R. K. Flitney, Seals and sealing handbook, Sixth edition. ed., Waltham, Massachusetts ;: Butterworth-Heinemann, 2014.

[8] J. Seewig and T. Hercke, "Lead characterisation by an objective evaluation method" *Wear,* vol. 266, p. 530–533, March 2009.

[9] T. Kunstfeld, Einfluss der Wellenoberfläche auf das Dichtverhalten von Radial-Wellendichtungen, Stuttgart: IMA, 2005.

[10] F. Guo, X. Jia, Z. Gao and Y. Wang, "The effect of texture on the shaft surface on the sealing performance of radial lip seals" *Science China Physics, Mechanics and Astronomy,* vol. 57, p. 1343–1351, April 2014.

[11] P. C. Hadinata and L. S. Stephens, "Soft Elastohydrodynamic Analysis of Radial Lip Seals With Deterministic Microasperities on the Shaft" *Journal of Tribology,* vol. 129, p. 851–859, April 2007.

[12] W. Li, Experimental Benchmarking Of Surface Textured Lip Seal Models, University of Kentucky, 2012.

[13] S. Jung and W. Haas, "Erweiterte Beschreibung von Gegenlaufflächen für Radial-Wellendichtungen" *Proceedings of the 15th International Sealing Conference (ISC),* pp. 63-72, 2008.

[14] M. Narten, Abdichtung von fließfettgeschmierten Getrieben mit Radialwellendichtungen - Reibungsminderung durch Makrostrukturierung der Dichtungsgegenlauffläche, Stuttgart: IMA, 2014.

[15] K. H. Warren and L. S. Stephens, “Effect of Shaft Microcavity Patterns for Flow and Friction Control on Radial Lip Seal Performance–A Feasibility Study” *Tribology Transactions,* vol. 52, p. 731–743, October 2009.

[16] S. Thielen, P. Breuniger, H. Hotz, C. Burkhart, T. Schollmayer, B. Sauer, S. Antonyuk, B. Kirsch and J. C. Aurich, “Improving the tribological properties of radial shaft seal countersurfaces using experimental micro peening and classical shot peening processes” vol. 155, p. 106764, 2021.

[17] S. Thielen, B. Magyar and B. Sauer, “Thermoelastohydrodynamic Lubrication Simulation of Radial Shaft Sealing Rings” *Journal of Tribology,* vol. 142, p. 052301, 2020.

[18] A. Shinkarenko, Y. Kligerman and I. Etsion, “The effect of surface texturing in soft elasto-hydrodynamic lubrication” *Tribology International,* vol. 42, pp. 284-292, 2009.

[19] D. Keller, G. Jacobs and S. Neumann, “Development of a Low-Friction Radial Shaft Seal: Using CFD Simulations to Optimise the Microstructured Sealing Lip” *Lubricants,* vol. 8, p. 41, 2020.

[20] F. Guo, X. Jia, L. Wang and Y. Wang, “The effect of axial position of contact zone on the performance of radial lip seals with a texturing shaft surface” *Tribology International,* vol. 97, pp. 499-508, 2016.

[21] Y. Kligerman and A. Shinkarenko, “The effect of tapered edges on lubrication regimes in surface-textured elastomer seals” *Tribology International,* vol. 44, pp. 2059-2066, 2011.

[22] R. Zhang, P. Steinert and A. Schubert, “Microstructuring of surfaces by two-stage vibration-assisted turning” *Procedia CIRP,* vol. 14, pp. 136-141, 2014.

[23] P. Steinert, A. Nestler, J. Kühn and A. Schubert, “Efficient Manufacturing of Tribological Surfaces by Turning Technologies with Alternating Movements” in *Proc. of International Conference on Competitive Manufacturing (COMA 16)*, Stellenbosch, 2016.

[24] P. Steinert, Fertigung und Bewertung deterministischer Oberflächenmikrostrukturen zur Beeinflussung des tribologischen Verhaltens von Stahl-Bronze-Gleitpaarungen, vol. 11, A. Schubert, Ed., Verlag Wissenschaftliche Scripten, 2017.

[25] R. Börner, S. Winkler, T. Junge, C. Titsch, A. Schubert and W.-G. Drossel, “Generation of functional surfaces by using a simulation tool for surface prediction and micro structuring of cold-working steel with ultrasonic vibration assisted face milling” *Journal of Materials Processing Technology,* vol. 255, pp. 749-759, 2018.

[26] R. Börner, M. Penzel, T. Junge and A. Schubert, “Design of Deterministic Microstructures as Substrate Pre-Treatment for CVD Diamond Coating” *Surfaces,* vol. 2, pp. 497-519, 2019.

[27] C. Burkhart, S. Thielen and B. Sauer, "Online determination of reverse pumping values of radial shaft seals and their tribologically equivalent system" *Tribologie und Schmierungstechnik,* vol. 67, 2020.

[28] H. Raab and W. Haas, "Tribologische Partner: Radialwellendichtring und Gegenlauffläche" *Antriebstechnik,* 1999.

[29] S. Thielen, T. Subramanian, B. Sauer, O. Koch, R. Börner, T. Junge and A. Schubert, "Characterisation of the conveying effect of turned radial shaft seal counter-surfaces using a simplified hydrodynamic simulation model" *Forschung im Ingenieurwesen,* vol. 87, p. 655–671, January 2023.

[30] S. Thielen, Entwicklung eines TEHD-Tribosimulationsmodells für Radialwellendichtringe, Als Manuskript gedruckt ed., Kaiserslautern: Technische Universität Kaiserslautern, 2019.

[31] T. Woloszynski, P. Podsiadlo and G. W. Stachowiak, "Efficient Solution to the Cavitation Problem in Hydrodynamic Lubrication" *Tribology Letters,* vol. 58, March 2015.

[32] D. Gropper, L. Wang and T. J. Harvey, "Hydrodynamic lubrication of textured surfaces: A review of modeling techniques and key findings" *Tribology International,* vol. 94, p. 509–529, February 2016.

8 Authors

Lenine M. de C. Silva, M. Sc.[1], ORCID 0000-0003-1272-0171, lenine.silva@rptu.de
Olaf Grutza, M. Sc.[1], ORCID 0009-0002-9776-093X, olaf.grutza@rptu.de
Prof. Dr.-Ing. Oliver Koch[1], ORCID 0000-0001-5967-0242, oliver.koch@rptu.de
Dr. -Ing. Stefan Thielen[2], ORCID 0000-0003-3310-7659, stefan.thielen@itwm.fraunhofer.de
Thomas Junge, M. Sc.[3], ORCID 0000-0002-0491-5190, thomas.junge@mb.tu-chemnitz.de
Dr. Andreas Nestler[3], ORCID 0000-0002-7355-793X, andreas.nestler@mb.tu-chemnitz.de
Prof. Dr.-Ing. Andreas Schubert [3], ORCID 0000-0002-7396-8413, andreas.schubert@mb.tu-chemnitz.de

[1] University of Kaiserslautern-Landau, Chair for Machine Elements, Gears and Tribology (MEGT)
Gottlieb-Daimler Straße, 67663 Kaiserslautern, Germany

[2] Fraunhofer Institute for Industrial Mathematics (ITWM)
Fraunhoferplatz 1, 67663 Kaiserslautern, Germany

[3] Chemnitz University of Technology, Professorship Micromanufacturing Technology
Reichenhainer Straße 70, 09126 Chemnitz, Germany

https://doi.org/10.61319/43PTY0VA